Stability and Reactivity of the Phenalene and Olympicene Isomers

Luiz F. A. Ferrão^{1*}, Marcelo A. P. Pontes¹, Gabriel F. S. Fernandes¹, Fernanda Bettanin², Adélia J. A. Aquino³, Hans Lischka^{4*}, Dana Nachtigallova^{5,6*}, Francisco B. C. Machado^{1*}

¹ Departamento de Química, Instituto Tecnológico da Aeronáutica, São José dos Campos, 122228-900, SP, Brazil

² Escola de Artes, Ciências e Humanidades (EACH) - Universidade de São Paulo (USP), São Paulo, 03828-000, SP, Brazil

³ Department of Mechanical Engineering, Texas Tech University, Lubbock, TX, 79409, USA

⁴ Department of Chemistry and Biochemistry, Texas Tech University, Lubbock, TX 79409-1061, USA

⁵ Institute of Organic Chemistry and Biochemistry, Academy of Sciences of the Czech Republic, Flemingovo nam. 2, CZ-16610 Prague 6, Czech Republic

⁶ IT4Innovations, VŠB-Technical University of Ostrava, 17. listopadu 2172/15, 70800 Ostrava-Poruba, Czech Republic

^{*}Corresponding authors: fmachado@ita.br, ferrao@ita.br, dana.nachtigallova@uochb.cas.cz, hans.lischka@ttu.edu

2

Abstract

The phenalene (triangulene) and olympicene molecules belong to the polycyclic aromatic

hydrocarbons (PAHs) class, which attracted substantial technological interest due to their unique

electronic properties. Electronic structure calculations serve as a valuable tool in investigating the

stability and reactivity of these molecular systems. In the present work, the multireference calculations,

namely the complete active space second-order perturbation theory (CASPT2) and multireference

averaged quadratic coupled cluster (MR-AQCC), were employed to study the reactivity and stability

of phenalene and olympicene isomers, as well as their modified structures where the sp^3 -carbon at the

borders were removed.

The harmonic oscillator model of aromaticity (HOMA) and the nucleus-independent chemical

shift (NICS) as geometric and magnetic indexes calculated with density functional theory were utilized

to assess the aromaticity of the studied molecules. These indexes were compared with properties such

as the excitation energy and natural orbitals occupation. The reactivity analyzed using the HOMA

index combined with MR-AQCC revealed the radical character of certain structures, as well as the

weakening of their aromaticity. Moreover, the results suggest that the removal of sp^3 -carbon atoms

and the addition of hydrogen atoms did not alter the π network and the excitation energies of the

phenalene molecules.

Keywords: Polycyclic aromatic hydrocarbons; Aromaticity; Radical character; Electronic structure

I. Introduction

Polycyclic aromatic hydrocarbons (PAHs) are important building blocks for organic semiconductors¹. Their extended π-conjugation electronic structures lead to large molar absorption coefficients, high quantum yields of photoluminescence, and excellent charge carrier mobilities², enabling their use in organic light-emitting diodes (OLEDs)^{3,4} and organic field-effect transistors (OFETs)^{5,6} with performance competitive with silicon-based electronic devices⁷. However, the selection of PAHs applicable in electronic devices is limited by the requirements for high product yield and long lifetime. For example, linear acenes comprising more than five benzene rings exhibit instability due to their low ionization potentials (IPs) and narrow band gaps^{8,9}. Therefore, considerable attention has been directed towards neutral radicals derived from planar polycyclic aromatic hydrocarbons wherein unpaired electrons delocalized through the carbon skeleton¹⁰. Examples include phenalenyl (Scheme 1), which has been synthesized previously by both a mass growth process¹¹ and a chemical route¹², as well as the more recently synthesized olympicenyl (Scheme 1)¹³. Investigations have also been performed on spin delocalization in open-shell PAHs derived from the helicene structure¹⁴.

Spin delocalization facilitates the self-assembly of these systems through multicentric couplings^{15–18}, resulting in a notable impact on their magnetic and conductive properties^{19–24}. The radical nature of peripheral carbon allows for its substitution, thereby enabling the control over spin properties and intermolecular interactions/packing during the synthesis of organic semiconductors^{25–27}. Due to the possibility of modifying and controlling the distribution of their spin densities, these systems serve as building blocks in the synthesis of nanostructures possessing an open-shell electronic structure.

The most extensively researched neutral radical PAH is phenalenyl^{12,28–30} (referred to as **I**), which consists of three planar hydrocarbon rings with 13 π -electrons (C₁₃H₉). The unpaired spin density is delocalized across six equivalent carbon atoms (Scheme 1, C-1, α -carbon atoms) exhibiting extended delocalization. This delocalization is also maintained in its cationic and anionic forms,

making **I** a versatile amphoteric redox system³¹. Due to these remarkable properties, **I** belongs to the group of molecular conductors, which are known for their electrical and magnetic bistability^{32–35} Compared to phenalenyl, much less research has been conducted on olympicenyl (referred to as **II**), which derives from triangulene. Unlike in phenalenyl, the spin density distribution is not uniform²⁷. Olympicenyl radicals have been identified using EPR spectroscopy^{36,37} and STM/AFM imaging³⁸. Theoretical studies mainly focused on understanding the adsorption behavior of olympicenyl radicals on surfaces^{39–42}. Notably, the crystal structure of olympicenyl radicals has been only recently resolved¹³ by detecting dimer structures, which co-exist in equilibrium with monomers in the solvent.

The hydrogenation of open-shell PAH radicals has emerged as a promising avenue for modifying their electronic and magnetic properties^{43–45}. Interestingly, these systems have been proposed as potential catalysts for hydrogenation reaction to form H₂ ^{46,47}. These studies also include hydrogenation of **I**, leasing to the formation of phenalene systems ^{48–50}.

Depending on the H-position, four possible isomers were investigated⁴⁹, among which only the 1H-phenalene was synthesized so far⁵¹. B3LYP calculations indicate that 1H-phenalene in the singlet state is the most stable, while the existence of 2H-phenalene in the triplet state is also suggested⁴⁹. The observed barrierless H-addition to I and a small barrier penetrable by tunneling for H-abstraction,⁴⁸ together with exceptionally weak C-H bond at the CH₂ moiety (260 kJ/mol as compared to 373 kJ/mol for analogous bonds in toluene¹¹) make the phenalenyl-based systems promising candidates for H-storage. Hydrogenation of II can form eleven isomers, characterized by either closed-shell or radical electronic structure. Calculations using a two-electron reduced density matrix (2-RDM) have predicted that although the latter are significantly less stable, they still exhibit stability with respect to the hydrogen dissociation.⁵²

Hydrogenated and additionally functionalized neutral hydrocarbon radicals offer great potential as materials for synthesis and can be further manipulated to form molecular organic switches with selective reactivity. Research on hydrocarbon radicals such as 1,14-dimethyl[5]helicene⁵³ and

13,14-dimethyl-centhrene⁵⁴ has introduced a novel concept for designing all-organic magnetic switches. These switches can be controlled by the ring opening/closure and facilitated by the UV/VIS light.

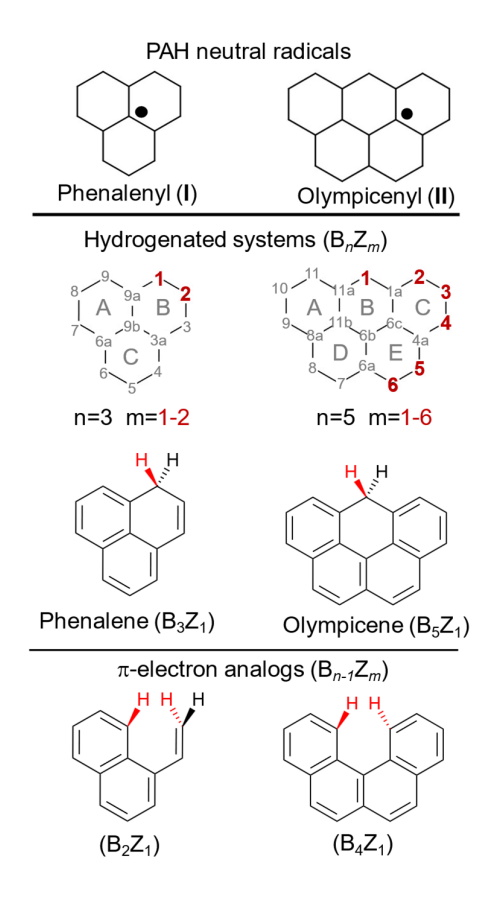
Although PAHs are recognized as promising photoactive materials due to their structural versatility and influence on the electronic structure, most of the studies on the excited states have focused on linear acenes. Other PAHs, especially those containing an odd number of carbon atoms, have received much less attention in research. There has been recent progress in calculating the low-lying excited states of the phenalenyl radical and its H-adducts. ^{50,55,56} These investigations shed light on the electronic properties and nature of the excited states of PAH cations ^{50,55,57,58} and anions ⁵⁹ with an odd number of carbon atoms, including phenalenyl and olympicene anions, have been studied as well, and the differences in the excited state behavior compared to systems with even-number of carbon atoms have been discussed ⁵⁹. To the best of the authors' knowledge, despite significant progress, there remains a gap in the systematic computationally based study on the specific properties, including the excited states, of these promising systems. The calculations are mainly based on the DFT approach. However, the radical character of the systems necessitates benchmarking of DFT methods through comparison with multireference wave-function-based methods. This ensures a more accurate and comprehensive understanding of their electronic properties and excited states.

The present study focuses on investigating the stability and aromaticity of phenalene, olympicene, and their isomers using DFT and multireference methods as benchmarks. Aromaticity indexes were used to characterize the studied systems, namely the Harmonic Oscillator Model of Aromaticity (HOMA) and the nucleus-independent chemical shift (NICS) indexes, calculated at geometries optimized at the DFT level. The multireference character and the occupation of the natural orbitals were analyzed using Multireference Averaged Quadratic Coupled-Cluster (MR-AQCC) calculations. The low-lying excited states were described with the Second-Order Complete Active Space Perturbation Theory (CASPT2). Analogous structures derived from the just-mentioned

compounds obtained by ring opening and carbon removal were also considered as possible alternatives for a systematic modification of open shell materials.

II. Methods

All the phenalene and olympicene isomers and π -electrons analogs are denoted herein as $B_n Z_m$, where n is the number of the six-carbon rings contained in the molecular structures investigated (n=2,3,4,5), and m labels the positioning of all non-equivalent hydrogen additions to a carbon atom of the phenalenyl and olympicenyl radicals, which are numbered following the convention for fused polycycles. The cases m=1-2 for the phenalene isomers and m=1-6 for olympicene isomers are presented in Scheme 1. The π -electron analogs were built based on the hypothesis that the position (m) of the out-of-plane hydrogen leading to an sp^3 -carbon in $B_n Z_m$, or the exclusion of the sp^3 -carbon at the same position followed by hydrogen passivation in $B_{(n-1)} Z_m$, should lead to the same π orbitals framework and, therefore, similar stability and aromaticity, as expected by their Clar structures foliations. The original, non-hydrogenated phenalenyl (Π) and olympicenyl (Π) radicals are also shown in Scheme 1.



Scheme 1. (Upper part) Molecular structures of phenalenyl (I) and olympicenyl (II) radicals; (middle part) their hydrogenated versions studied in the present paper, phenalene (B₃Z₁), olympicene (B₅Z₁), and its isomers (B_nZ_m); (lower part) π -electron analogs of phenalene and olympicene isomers ($B_{n-1}Z_m$). The middle part of the scheme defines the position of the out-of-plane hydrogen (m) of the hydrogenated systems and, therefore, of the sp³ carbon, which is removed in the analogs. The numbering of the carbon atoms is in red for all the non-equivalent positions studied and in grey for other redundant and graphitic carbons. The molecular structures of all studied molecules are shown in Scheme S1 in the supporting information.

All molecules were optimized using Density Functional Theory (DFT) within the B3LYP⁶² functional combined with the 6-31G* basis set^{63,64} for both singlet and triplet multiplicities (see the Cartesian Coordinates in the Supporting Information). To validate this methodology, geometry optimizations of the three-ring systems (B_3Z_1 and B_3Z_2) were also caried out using M06-2X/def2-TZVP

^{65–67}. The aromatic character of the studied systems was calculated from the B3LYP/6-31G* optimized geometries according to the HOMA analysis⁶⁸,

$$HOMA = 1 - \frac{\alpha}{n} \sum (R_{Opt} - R_i)^2 \tag{1}$$

where n is the number of carbon-carbon bonds in the ring (n = 6 in this work), α is a parameter that depends on the atomic species involved in the chemical bond ($\alpha_{C-C} = 257.7 \text{ Å}^{-2}$), Ro_{pt} is the optimal bond value (1.388 Å for CC bond), that, for an ideal aromatic system (HOMA = 1.0), the calculated bond length, R_i , should be equal to Ro_{pt} . For HOMA equal to 0.0, the ring system should have a non-aromatic Kekulé structure, alternating the geometry with single and double bonds. The HOMA index was calculated using the pyCRAI code.^{69,70} The Nucleus-Independent Chemical Shifts (NICS) calculations were also used to identify the aromatic character of the studied systems. The NICS is given by the negative of the spherically averaged magnetic shielding tensor⁷¹,

$$NICS(R) = -\frac{1}{3}tr[\underline{\sigma}(R)] = -\frac{1}{3}(\sigma_{xx}(R) + \sigma_{yy}(R) + \sigma_{zz}(R))$$
 (2)

in which the magnetic shielding $(\underline{\sigma}(R))$ is a 3 x 3 tensor field that relates an applied external magnetic field (B_{ext}) and an induced magnetic field (B_{ind}) at a given point in space R,

$$B_{ind}(R) = -\underline{\sigma}(R)B_{ext} \tag{3}$$

The shielding tensor matrix elements $(\sigma_{\gamma\beta}(R))$ can be evaluated as the mixed second derivative of the energy with respect to an external magnetic field (B_{β}) . The nuclear magnetic moment (μ_{γ}) is usually given in parts per million (ppm), *i.e.*, the magnitude of the induced field is typically in the order of a million times weaker than the applied field.

When measured 1 Å above the plane of a ring lying in the xy plane in which the origin is at the center of the ring, *i.e.*, R = (0,0,1), the NICS value is usually denoted as NICS(1). For benzene, the NICS(1) value (~ -10 ppm) is dominated by the σ_{zz} term (~ 30 ppm), giving a reference value for the magnetic shielding of an aromatic system. As a counter-example, the cyclobutadiene presents a

NICS(1) value ($\sim +17$ ppm) which is also dominated by the σ_{zz} term (~ -51 ppm), giving a reference value for the magnetic deshielding of an anti-aromatic system.

In the present study, two approaches were used to investigate the NICS values of the studied systems. First, the NICS was calculated not only at the center of the ring but for several (x,y) positions 1 Å above the plane of the molecule, *i.e.*, R = (x, y, 1). This NICS(XY1) indicates the aromatic regions in planar molecules, and hereinafter, these NICS(XY1) "heat maps" will be referred to simply as NICS(1). It is worth noting that some molecules studied are not fully planar, so the NICS(1) of such molecules will represent slightly different z distances, depending on the x,y position. The second approach consisted in calculating the NICS values along a line orthogonal to the molecular plane and passing through the center of the ring with different distances from the plane, *i.e.*, R = (0,0,z). These are denoted NICS(z) scans in the present paper. The NICS(z) scans were calculated for the π -only system by subtracting the σ -only isotropic component from the total isotropic system^{72,73}. The probe atom (Bq) was positioned with z values from 0 to 3.9 Å.

Also, to access the relative importance of the various matrix elements of the shielding tensor, we used the visualization of the chemical shield tensor method (VIST)^{71,74}, as implemented in the TheoDORE package⁷⁵, in which the principal axes of the shielding tensor ($q^{(i)}$; i = 1,2,3) at a given point in space (R) are determined via an eigenvalue decomposition ($t^{(i)}$) and subsequently visualized via dumb-bells whose sizes depend on the size of the associated eigenvalue. In this local coordinate system, the sum of the eigenvalues in the three principal axes also returns the NICS values in an equation equivalent to Eq. (2):

$$NICS(R) = -\frac{1}{3}tr[\underline{\sigma}(R)] = -\frac{1}{3}(t^{(1)}(R) + t^{(2)}(R) + t^{(3)}(R))$$
(4)

All VIST calculations were carried out for R = (0,0,1). Also, all NICS(1) heat maps, NICS(z) scans, and VIST were obtained with single-point B3LYP/6-311+G* methodology.

Single-point MR-AQCC calculations⁷⁶ were used to obtain the occupation of the natural orbitals and the singlet-triplet separation energy. The complete active self-consistent field (CASSCF)⁷⁷

wave function was constructed, including electronic configurations within the spatial symmetry and spin multiplicity allowed. The active space used was CAS(8,8), *i.e.*, eight electrons in eight π orbitals, since it is known that the low-lying electronic states of acenes and periacenes usually possess two main singlet transitions involving up to four occupied and four virtual frontier orbitals⁷⁸. 6-31G* basis set was used for these calculations.

For the higher-symmetry three-ring systems (B_3Z_1 and B_3Z_2), the low-lying electronic states were further treated with single-point calculations through a multireference perturbation theory to the second-order (SS-CASPT2)⁷⁹⁻⁸⁴, which uses the CASSCFas the zero-order wave function. The orbitals for the active space were chosen based on the complete π space (12,12). The reference space for the dynamical correlation step was chosen as a subset of the complete π space, including all the configuration state functions (CSFs) generated from a CASSCF(4,4)RASSCF(8,8), considering single and double excitations in the restricted space. To calibrate the methodology, we compared the singlet-triplet energy separations to those obtained with MR-AQCC/CASSCF(8,8). This calibration also included a comparison between the 6-31G* basis set with the more extended basis def2-TZVP^{66,67}. All 1s orbitals of all molecules were kept frozen. In the CASPT2 calculation, a level shift (0.2 a.u.) was included to remove possible intruder states in the excited states calculations⁸⁵. The core orbitals were also kept frozen in these calculations. All the geometry optimizations were performed using the Gaussian 09 package, and the single-point multiconfigurational calculations were carried out using Molpro 2015. ^{87,88}

The electronic structure differences between the PAH isomers were studied by calculating the singlet-triplet energy separation and characterizing the low-lying electronic states of each system at the ground state geometry using the MR-AQCC//B3LYP/6-31G* approach. The multiconfigurational character of the systems was determined by the largest squared coefficient (C_0^2) of the configurations in the CASSCF wavefunction, representing the weight of a single electronic configuration in the total wavefunction.

III. Results

Prior to discussing the results for the molecules that are the objective of the present paper, benzene and coronene were characterized using the same methodology. This analysis aims to verify the reliability of the computational approach in obtaining CC bond lengths and to calibrate the sensibility of the calculated aromatic indicators to these bond lengths. The coronene system can be used as a reference fully aromatic system constructed from fused benzene rings. The results of the different analysis methods (HOMA, NICS(1), and VIST) are summarized in Figure 1. It is worth noting that similar NICS(1) analyses have been performed previously for these reference systems^{89,90}. The CC distances in benzene, calculated as 1.397 Å, differ by less than 0.001 Å from the experimental values⁹¹, leading to an aromatic model with a HOMA index of 0.98. For coronene, the calculated bond distances for peripheral double bonds (1.372 Å) agree within 2% with the experimental values⁹² (average of 1.343 Å). For the central spoke bonds the calculated value (1.4275 Å) presents a much lower error (0.4%) when compared to the experimental data (average of 1.422 Å). 92 The resulting HOMA index values of the central and outer rings are 0.60 and 0.71, respectively. These observations correspond to trends in NICS(1) and VIST values. The values of coronene show that the outer rings exhibit larger aromaticity, comparable to that of the benzene ring, while the central ring displays lower aromaticity. The eigenvalues of the magnetic shielding tensor, as revealed by the VIST method, indicate the prevalence of the out-of-plane component in the chemical shielding tensor for both systems.

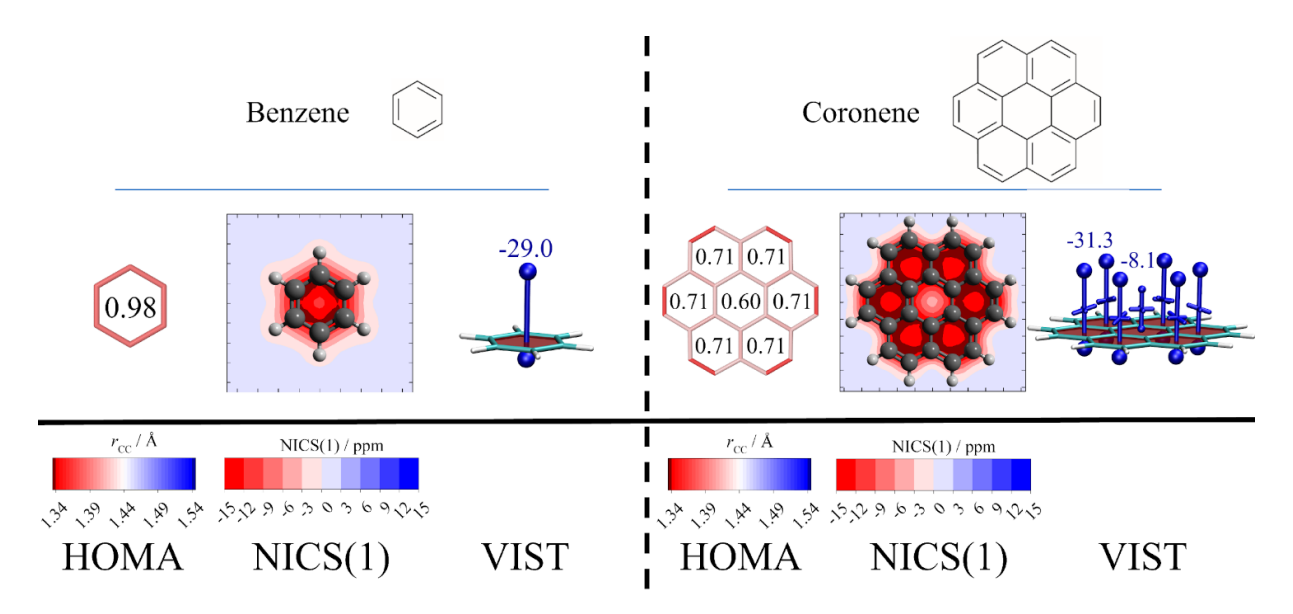


Figure 1. Characterization of aromaticity of reference systems (benzene and coronene) through geometric (HOMA) and magnetic indexes (NICS), accompanied by the visualization of the shielding tensor method (VIST). Color scales are presented for the bond lengths and NICS(1) values, while the eigenvalue of the dominant contribution of the chemical shielding is present for each ring. The HOMA values are presented inside each ring.

A. Phenalene isomers and π -electron analogous

Figure 2 illustrates the C-C bond distances of the optimized B₃ systems, their related B₂ systems, possible resonance structures, and the aromatic indicators HOMA, NICS(1), and VIST. The presence of the CH₂ group in *1H*- and *2H*-phenalene disrupts the extended aromaticity, which is the cause of the remarkable stability of phenalenyl and its cation and anion. The bond distances and their changes in the non-substituted rings A and C, which constitute a naphthalene-like fragment, are similar to coronene. Changes in the C-C bond distances that involve sp³-hybridized carbon atoms vary significantly depending on the specific site of the hydrogen addition. In B₃Z₁, the disruption of aromaticity results in the elongation of C1-C9a (1.52 Å) and C1-C2 bonds (1.50 Å), both of which correspond to a single C-C bond and localization of single and double bonds to C3-C3a (1.47 Å) and C2-C3 (1.34 Å), respectively. In B₃Z₂, the elongation of the bonds connecting the sp³-hybridized C2

is analogous (1.47 Å for C2-C1 and C2-C3), while C1-C9a and C3-C3a correspond to aromatic bonds with distances of 1.40 Å. The bond properties discussed above for B_3Z_1 and B_3Z_2 do not qualitatively change if the sp^3 carbon atoms are removed from the system to form B_2Z_1 and B_2Z_2 .

The resonance structures in Scheme 1 and Fig. 2 show that both systems retain the aromatic character on the naphthalene-like fragment formed by rings A and C. The different localization of the sp³ carbon atom is reflected in the different electronic structures of the B ring in B₃Z₁ and B₃Z₂. The analyses of the ground-state wavefunctions (see Table S1 for CI coefficients and electronic configurations) show that while the resonance structures of the former correspond to a closed shell, the latter is biradical. The analyses of the orbital occupation of the frontier orbitals using MR-AOCC and their orbital plots are presented in Figure 3 and S1, respectively. The occupation numbers of the highest occupied natural orbital (HONO) and lowest unoccupied natural orbital (LUNO) of B₃Z₁ are 1.92 e and 0.08 e, respectively. In comparison, the HONO and LUNO of B₃Z₂ have occupation values around 1.4 e and 0.6 e, Z₂, respectively. The orbital plots (Figure S1) show a strong delocalization in B₃Z₂, suggesting that the radical character extends over the entire molecule. The radical nature of this structure is the reason for the lower stability of this system. The ground state of the 2H-phenalene molecule (B₃Z₂) was previously calculated as a triplet open-shell structure⁴⁹, lying 19.4 kcal mol⁻¹ below the singlet structure, which indicates its radical character and difficulty for experimental detection. According to our calculations (see Figure 5 and Table S2), B₃Z₁, with a larger aromatic character, is by 1.54 eV more stable than B₃Z₂, and its singlet/triplet gap is significantly larger.

Removal of sp³-carbon only contributes to the changes within the framework of σ -orbitals; it should not change the electronic structure of the frontier orbitals of the PAHs isomers (formed by π -orbitals). Thus, the out-of-plane position of hydrogen (m) leading to the sp³-carbon in B_nZ_m or the exclusion of the sp³-carbon at the same site with subsequent hydrogen passivation in $B_{(n-1)}Z_m$ should lead to the same electronic structure within the π -orbital framework and thus to similar stability and aromaticity. This behavior corresponds to Clar's structures and almost identical HONO and LUNO

occupation numbers of B_nZ_m and $B_{(n-1)}Z_m$ when (m) is the same (Figure 3). Orbital plots of HONO and LUNO of all two- and three-ring systems (Figure S1) show a strong delocalization, suggesting that in the B_3Z_2 and B_2Z_2 , the radical character extends over the entire molecule.

HOMA indices (Fig 2) calculated for the singlet-optimized structures show that for *1H*-phenalene, the aromaticities of A and C rings are almost comparable to those of the outer rings of coronene. In contrast, HOMAs of A and C in *2H*-phenalene are smaller and similar to the aromaticity of the central coronene ring. The lower HOMA values for the latter are due to the delocalization of the radical character in these rings, as indicated by the HONO and LUNO orbital plots.

HOMA analysis gives a different picture for geometries optimized in the triplet state (also in Fig 2). In B_3Z_1 , the HOMA index of ring A increases slightly while the HOMA index of ring C decreases significantly, indicating that the latter carries the open-shell character. On the other hand, the HOMAs of both rings of A and C rings in B_3Z_2 are slightly increased compared to the singlet-optimized structure, indicating increased aromaticity of the naphthalene fragment. It is worth mentioning that the HOMA results are similar while optimizing B_3Z_1 and B_3Z_2 utilizing M06-2X/def2-TZVP (refer to cartesian coordinates in the supporting information).

In B_2Z_1 , the reduction in aromaticity of the C ring is even more pronounced. The HOMA index suggests that the system in triplet geometry is completely non-aromatic. The new reparametrized HOMA for triplet states (HOMER) 93 corroborates these data. Using this reparameterization, the B_3Z_2 triplet state exhibits HOMER values of -0.14, -0.60, and -0.14 for the A, B, and C rings correspondingly. A constant slight decrease in aromaticity in the B_2Z_2 molecule compared to B_3Z_2 leads to almost identical aromaticity of the naphthalene fragment in the singlet and triplet geometries.

The HOMA values of the B ring in B₃Z₁ and B₃Z₂ provide only indicators of the stability of these systems rather than information on the aromaticity/non-aromaticity since this ring does not represent a fully conjugated system. In this case, HOMAs of -0.78 and 0.03 in the case of B₃Z₁ and of

B₃Z₂, respectively, point to the formation of two stable single bonds in the former and a less stable biradical with partial double bond character in the latter.

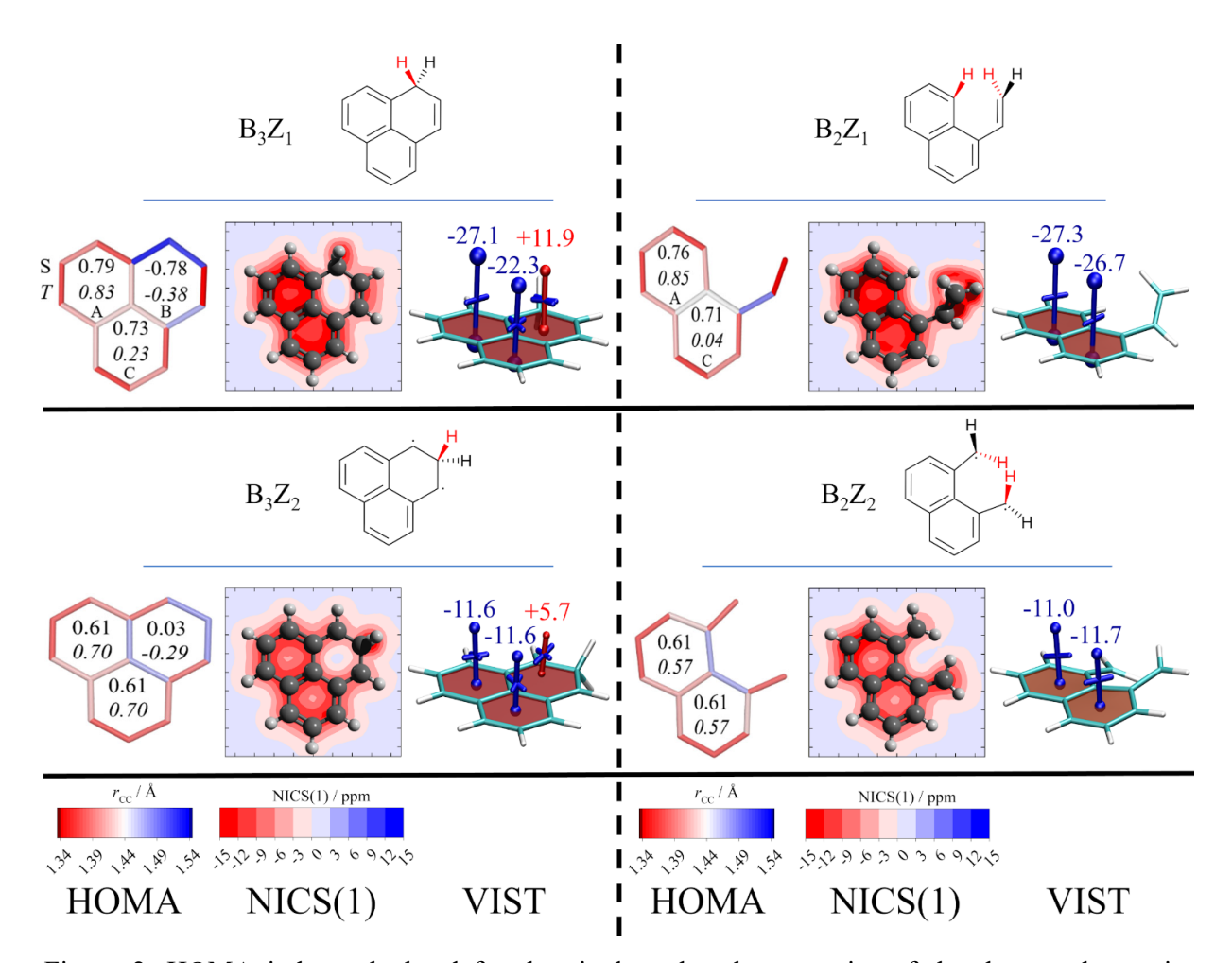


Figure 2. HOMA index calculated for the singlet relaxed geometries of the three and two-ring molecules. The color scale of the bond length shows the double carbon bond (1.34 Å) in red and the single carbon bond (1.54 Å) in blue for the singlet state. The numbers shown in the first and second lines inside each ring are the HOMA for the singlet and triplet optimized states, respectively. The NICS surfaces calculated around 1.0 Å above the *xy*-plane (NICS(1)) of the singlet (m=1) and triplet (m=2) B₃ and B₂ systems.

The analyses based on NICS (see Figure S2 for NICS(z) scans and Figure 2 for NICS(1), respectively) and VIST calculations (Figure 2) provide further support for the view on aromaticity discussed above. B_3Z_m and B_2Z_m present the same pattern for a given m, with NICS(1) values of the

unsubstituted A and C rings closer to those of benzene for m=1, while the NICS(1) values for m=2 are smaller in absolute value. The out-of-plane dominant contribution of the chemical shielding is also similar for B_3Z_m to B_2Z_m . The stable singlet systems present a dominant component with an eigenvalue of about -27 ppm and -11 ppm for the unsubstituted rings in systems with m=1 and m=2, respectively, and +11.9 ppm for the substituted one. The substituted ring (B in Scheme 1) presents a positive but smaller eigenvalue. It is important to note that the NICS(1) and VIST values of the substituted rings of B_3Z_m molecules should not be regarded as an anti-aromatic character. The deshielding associated with these rings is much more related to the breakage of the π -electron structure in these rings, as shown by the almost equivalence of the analogous B_2Z_m structures.

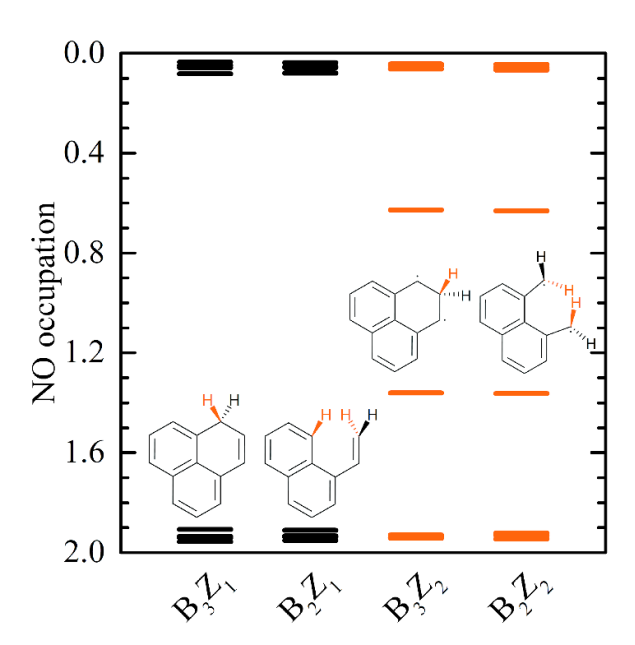


Figure 3. Frontier natural orbitals occupation obtained from MR-AQCC calculations for the three and two-ring systems.

A.I.I. Excited states of the phenalene isomers and π -electron analogous

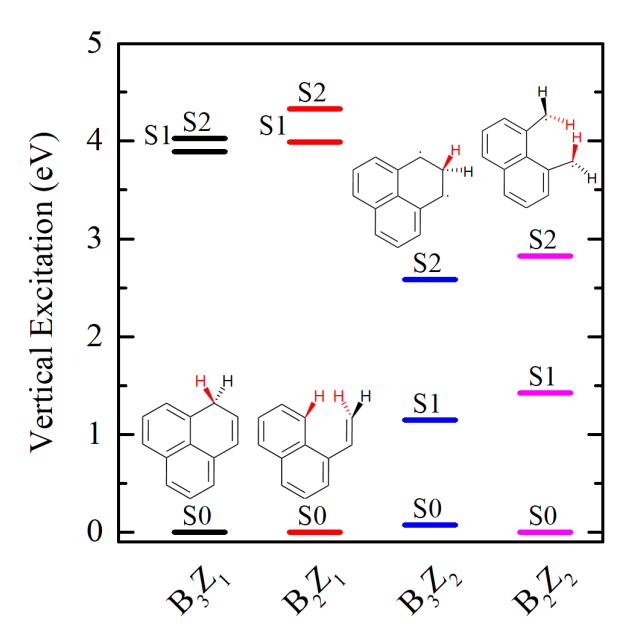


Figure 4. Vertical excitation energy scheme of the phenalene systems and their analog molecules obtained by the CASPT2(8,8)//B3LYP/6-31G* methodology. The methodology's calibration is available within the Supporting Information (Table S3).

Table S1 collects the most important electronic configurations of B_3Z_m species and their B_2Z_m modifications. As anticipated, the two lowest excited states of B_3Z_1 are analogous to those of naphthalene, i.e., the first two excited states are due to the HOMO \rightarrow LUMO+1 + HOMO-1 \rightarrow LUMO, and HOMO \rightarrow LUMO transitions, respectively. The excitation energies of these states are 3.89 and 4.03 eV (see Figure 4), in good agreement with the X-MCQDPT2 calculations (3.53 eV and 3.75 eV)⁵⁰ and experimental data (3.66 eV and 3.83 eV)⁵⁰. Note that these values are significantly higher than those of the corresponding phenalenyl neutral radical, for which the vertical excitation energy S1 calculated with the B3LYP/6-31G* method is 2.76 eV ⁵⁶. The corresponding excited states in B2Z1 shift to higher values by only 0.12 eV, confirming the previously discussed argument that the aromatic character does not change upon the removal of sp³-carbon. The ground and low-lying singlet states of B_3Z_2 present a multiconfigurational character (see Table S1) with low excitation energies

(1.05 eV and 2.21 eV for S₁ and S₂, respectively), as expected from its radical character. These values increase by about 0.4 eV in B₂Z₂, showing a slight decrease in its radical character.

In light of the correspondence of aromatic character with naphthalene discussed above, it is interesting to compare the excitation spectra of B_nZ_m with that of naphthalene. Its calculated excitation energies are 3.99 eV for S_1 (HOMO \rightarrow LUMO+1 and HOMO-1 \rightarrow LUMO) and 4.45 eV for S_2 (HOMO \rightarrow LUMO). Based on these results, it can be concluded that the aromaticity of naphthalene remains practically the same due to H-addition at C1. At the same time, substitution at C2 significantly affects this aromaticity.

B. Olympicene isomers and π -electron analogous

The relative stability of olympicene isomers calculated with MR-AQCC for the first singlet and triplet state of each system are shown in Figure 5. The total energy of all systems calculated with MR-AQCC and B3LYP methods is collected in Table S2. The MR-AQCC and B3LYP results (Figure 5, Table S2, and Table S3) differ significantly. In particular, the relative energies calculated with B3LYP are up to 0.41 eV (singlets) and 0.84 eV (triplets) lower than those obtained with MR-AQCC. However, both methods give the same ordering for the conformer stability in both spin multiplicities, with S₀(B₅Z₁) being the most stable among the olympicene isomers; B₅Z₄, B₅Z₂, and B₅Z₅are less stable by approximately 0.31, 0.39, and 1.2 eV, respectively.

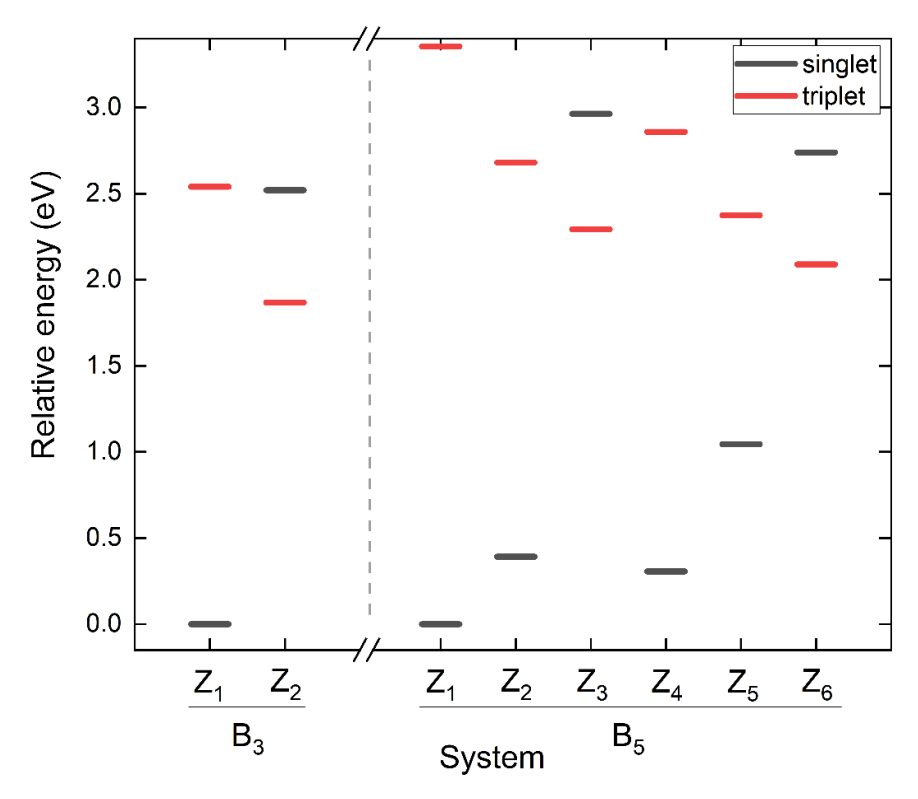


Figure 5. Relative energies (in eV) of isomers of phenalene (B_3Z_m) and olympicene (B_5Z_m). The levels in black refer to singlet states, while red refers to triplet states. The energies are obtained with MR-AQCC/6-31G*//B3LYP/6-31G*. (see Table S2 in the supporting information)

The singlet ground state wavefunction of all these structures has a dominant contribution from a closed-shell configuration (Figure S5), with a squared coefficient ($C\sigma^2$) of the main configuration in the MR-AQCC singlet wavefunction close to 90% for B₅Z_m (m=1,2, and 4) and of 87% for B₅Z₅. The occupation numbers of frontiers natural orbitals obtained by MR-AQCC and shown in Figure 6 follow the same trend; HONO/LUNO occupations are 1.93/0.05 for B₅Z₁, 1.92/0.06 for B₅Z₂, 1.92/0.07 for B₅Z₄, and 1.89/0.10 for B₅Z₅, respectively. In line with these results, the singlet/triplet energy gaps, calculated at the MR-AQCC level, are in the range of 2.2 – 3.5 eV for B₅Z_{1,2,4} (m=1,2, and 4) structures and 1.37 eV for B₅Z₅. In the case of B₅Z_m (m=3 and 6), the singlet/triplet energy ordering reverses, and the triplet becomes by 0.65 eV more stable than the singlet. The B3LYP method overestimates the relative stability of triplet states in all cases, lowering the singlet/triplet gap in all radical-free systems (Table S2).

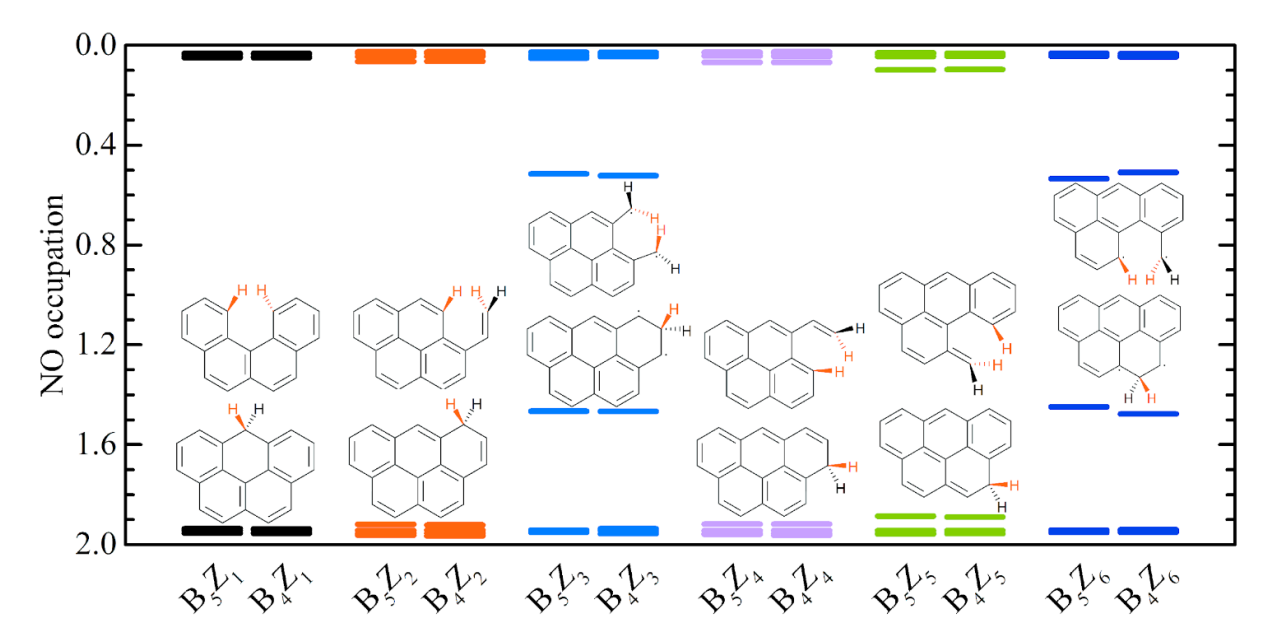


Figure 6. Frontier natural orbitals occupation obtained from MR-AQCC calculations for the five and four-ring systems. (The plots of the frontier natural orbitals are shown in Figure S3)

The wavefunctions of the lowest singlet states of B_5Z_3 and B_5Z_6 are strongly multiconfigurational, as shown by all relevant parameters; the CI coefficient values of the leading electronic configurations are about 0.64 (Fig. S5), and the occupation numbers of HONO and LUNO are about 1.6 and 0.4, respectively, giving these structures radical character. The corresponding energies of these states are in line with their radical character, being less stable by 2.96 (B_5Z_3) and 2.74 eV (B_5Z_6) at the MR-AQCC level (2.55 and 2.34 eV at the B3LYP level).

Figure 7 displays the C-C bond distances and HOMA indexes obtained from the geometries optimized at the B3LYP level for both multiplicities. For the most stable singlet olympicene (B₅Z₁), the HOMA values are similar to those calculated using the X-ray crystallographic structure for the olympicenyl radical¹³ for A and C rings, with differences around 0.06 for D and E rings (see Scheme 1 for ring labeling). All four rings in conjugation, i.e., A, C, D, and E, have HOMA indexes similar to those in coronene, showing strong aromaticity. As in the B₃Z₁, the HOMA of the substituted B ring is strongly negative. In the triplet state, the HOMA of A and C rings do not significantly change and

reduce for D and E rings, resulting in a significant reduction of the average HOMA value from 0.75 to 0.55. Also, the HOMA of ring B is less negative. B_5Z_2 , B_5Z_3 , and B_5Z_4 systems, with sp^3 carbon located at the C ring, can be viewed as substituted pyrene formed by A, B, D, and E rings. The calculated bond distances and HOMA values show that in the closed-shell B_5Z_2 and B_5Z_4 , the overall aromaticity preserves the symmetry and HOMAs close to pyrene. In the open-shell B_5Z_3 , the symmetry of HOMAs breaks, and the values are generally lower, both showing a partial delocalization of the radical character. These patterns are not preserved in the triplet state, and no apparent trends in changes from the singlet can be derived. However, the average HOMA only slightly decreases in B_5Z_2 and B_5Z_4 and increases in B_5Z_3 . B_5Z_5 , the least stable among the closed-shell isomers, and open-shell B_5Z_6 , both with the sp^3 carbon located on the D ring, feature the electronic structure with A, B, C, and D rings in conjugation. The HOMAs of the former show the least aromatic character among all calculated singlets due to the non-aromaticity of the D ring (HOMA = 0.16). In the latter, all conjugated rings show relatively high aromatic character with HOMA indexes close to those of coronene. These pictures do not change significantly in the triplet states of both systems, whose average HOMA indexes are larger (0.69 in B_5Z_5 and 0.70 in B_5Z_6) than in singlet states (0.54 in B_5Z_5 and 0.64 in B_5Z_6).

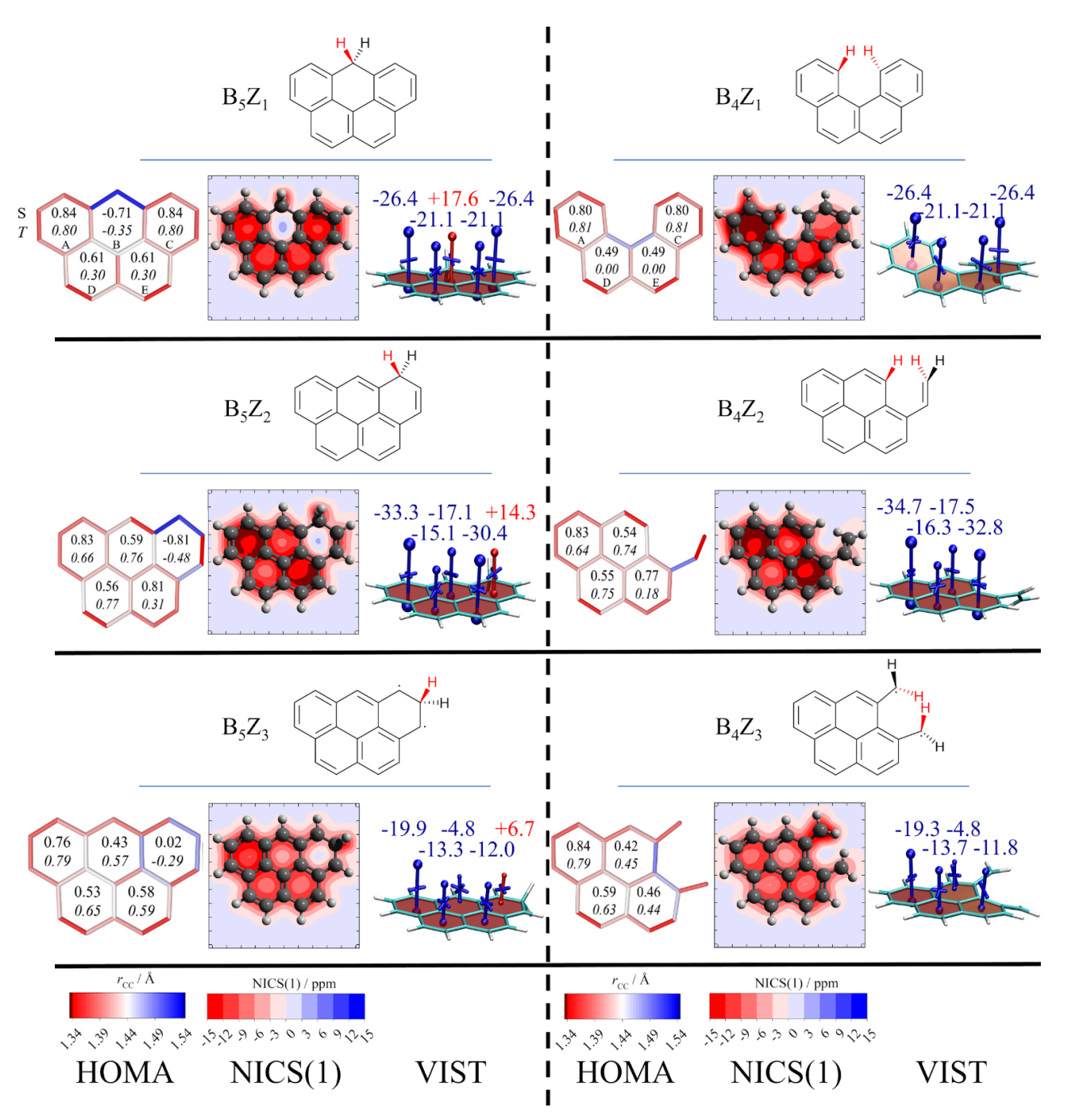


Figure 7. HOMA index calculated for the singlet relaxed geometries of the three- and two-ring molecules. The color scale of the bond length shows the double carbon bond (1.34 Å) in red and the single carbon bond (1.54 Å) in blue. The numbers shown in the first and second lines inside each ring are the HOMA for the singlet and triplet optimized states, respectively. The NICS surfaces were calculated around 1.0 Å above the *xy*-plane (NICS(1)) of the singlet (m=1, 2, 4, 5) and triplet (m=3, 6) B₅ and B₄ systems.

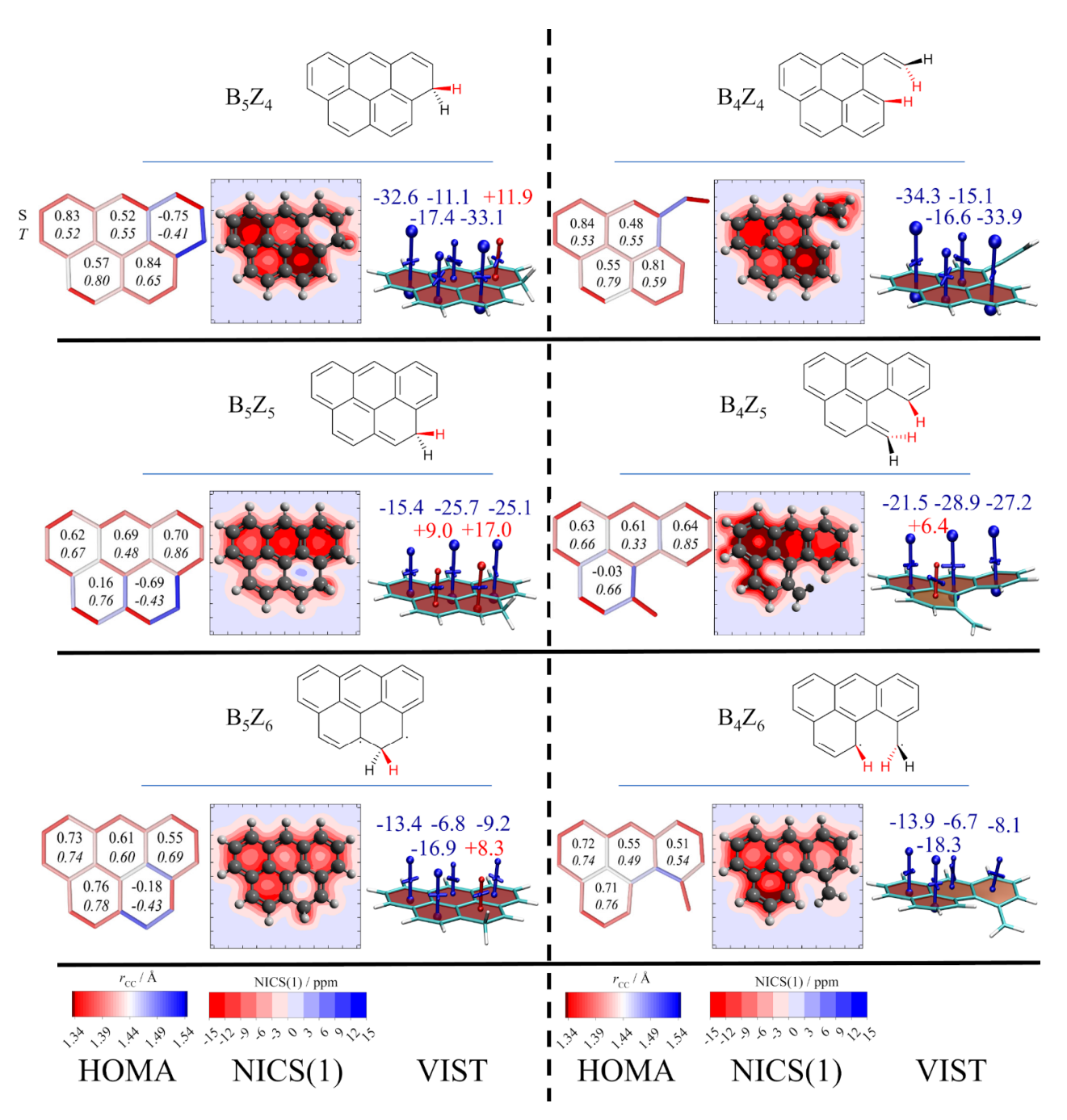


Figure 7. (continuation) HOMA index calculated for the singlet relaxed geometries of the three and two-ring molecules. The color scale of the bond length shows the double carbon bond (1.34 Å) in red and the single carbon bond (1.54 Å) in blue. The numbers shown in the first and second lines inside each ring are the HOMA for the singlet and triplet optimized states, respectively. The NICS surfaces were calculated around 1.0 Å above the *xy*-plane (NICS(1)) of the singlet (m=1, 2, 4, 5) and triplet (m=3, 6) B₅ and B₄ systems.

It would be interesting if an average of the HOMA values could return and correctly rank the stability of the studied species. A first approach would be to take the mean arithmetic value of all unsubstituted rings, which we called \overline{HOMA} in the present study. The \overline{HOMA} presents a fair correlation with other stability indexes discussed before, such as the relative energy or the natural orbital occupation, but wrongly predicts that B_3Z_6 to be among the stable isomers (values collected in Table S4). Since the \overline{HOMA} is not able to completely classify the studied systems from the most stable to least stable, we propose to represent the global HOMA ($\langle HOMA \rangle$) of such fused ring systems by using a weighted geometric mean with empirical values for the weights as follows,

$$\langle HOMA \rangle = (\prod_{i=1}^{n} HOMA_i^{w_i})^{\frac{1}{\sum_i w_i}} \qquad w_i = \begin{cases} 1, & \text{if } HOMA_i > 0 \\ 2, & \text{if } HOMA_i < 0 \end{cases}$$
 (5)

where the index (*i*) in Eq. 5 refers to a given ring, and the weights are doubled for the rings with negative HOMA values, which are the substituted rings for the studied systems. This equation interprets a hypothetical perfectly anti-aromatic ring (HOMA= -1) among perfectly aromatic rings, (HOMA = 1) just as a spacing between aromatic rings, without lowering the aromaticity of the system as a whole (only locally). This interpretation agrees with previous studies showing the aromaticity of accenes with the inclusion of a cyclobutadiene linkage, in which the system behaves as two smaller accenes spatially separated by the cyclobutadiene linkage.⁷⁰ The (HOMA) values, collected in Table S4, of the olympicene isomers are around 0.70 for B₅Z₁, B₅Z₂ and B₅Z₄, 0.53 for B₅Z₅, 0.43 for B₅Z₆ and 0.29 for B₅Z₃, which closely resembles the relative stabilities of the isomers. Figure 8 collects these two average HOMA values (\overline{HOMA} and (HOMA)) alongside the singlet-triplet energy separation of phenalene and olympicene isomers.

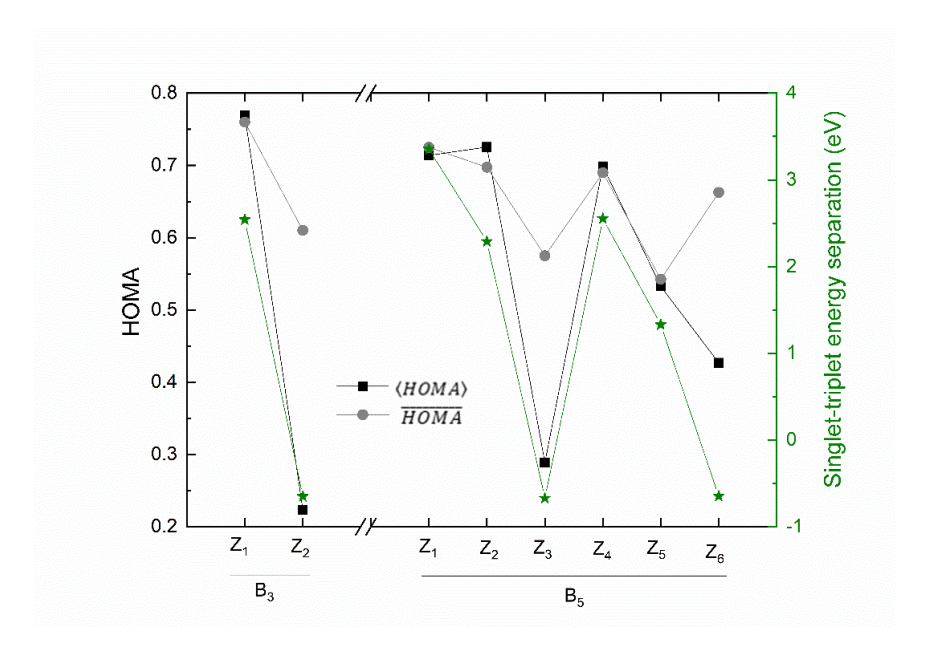


Figure 8. Global HOMA values and singlet-triplet energy separation (in eV) of isomers of phenalene (B₃Z_m) and olympicene (B₅Z_m). The values in black refer to the proposed weighted geometric mean ($\langle HOMA \rangle$, see Eq.5), while gray refers to the arithmetic mean (\overline{HOMA}). The energies are obtained with MR-AQCC/6-31G*//B3LYP/6-31G*.

Similar to phenalene-based systems, by removing the sp³ carbon atom to form B_4Z_m species, the character of the electronic states retain their single- and multiconfigurational characters. This preservation is supported by the CI coefficients of the leading electronic configuration (Fig. S5) and the relative singlet/triplet energy gaps (Fig. S5). A slight decrease is observed when comparing the HOMA indexes of B_4Z_m with the corresponding B_5Z_m molecules in both singlet and triplet states. These findings suggest that the electronic properties remain unaffected by the presence of sp³ carbon atoms, which are not part of the conjugated systems. The reduction in HOMA values mentioned above can mainly be attributed to the spatial deformation of the molecule, which tends in some systems to form helicoidal structures. Overall, the properties of the olympicene B_5Z_m and B_4Z_m molecules exhibit similarities to the phenalene B_3Z_m and B_2Z_m molecules. For m=1, 2, 4, and 5), the ring containing the substituted carbon displays a significantly negative HOMA value (ranging from -0.69 to -0.81), indicating stable molecules. For m=3 and 6, the biradical structures have HOMA values close to zero

(0.02 and -0.18), indicating unstable molecules. The position m =5 represents an intermediate scenario in terms of aromaticity, where the ring adjacent to the substituted D ring also possesses a HOMA value closer to zero (0.16 in B_5Z_5). In contrast, the substituted ring presents a HOMA of -0.69.

The analyses based on NICS and VIST calculations also support the view on aromaticity obtained from the HOMA index. The NICS(z) scans of B₅ and B₄ systems are presented in the supporting information (Figure S4). Counting the rings with higher aromaticity within NICS (1) and VIST values in Figure 7 also leads to the same general conclusions, in which m =1 seems to present four rings with high aromaticity, followed by m =2, 4, and 5, with two higher-aromaticity rings. For the biradical structure with m = 3, only one VIST value is reasonably negative (-19.9 ppm), located at the outermost ring; its position correlates well with the location of the largest HOMA. For the other biradical structure, m = 6, the VIST values indicate two moderately aromatic rings, in agreement with the HOMA analysis.

IV. Conclusions

In this study, *ab initio* methodologies were employed to investigate the reactivity and stability of phenalene and olympicene isomers, along with their sp^3 -carbon-modified structures. The calculated HOMA indexes indicated no significant changes when comparing B_3Z_m and B_5Z_m with their analogous models, B_2Z_m and B_4Z_m , respectively. This suggests that removing sp^3 -carbon of three and five-ring molecules does not affect the electronic structure. However, this index was able to signal important variations in the stability of phenalene (B_3Z_m) and olympicene (B_5Z_m) isomers to distinguish between two different classes of isomers in terms of the stability due to the modified rings by sp^3 -carbon.

The substituted rings with HOMA values more negative than – 0.6 were associated with stable molecules, while those with values closer to 0.0 indicated reactive isomers. To quantify this behavior, a weighted geometric mean was employed to represent the global aromaticity of these fused ring systems. MR-AQCC calculations provided further confirmation of this trend, as the HONO/LUNO

orbitals and the singlet-triplet separation energy exhibited radical character for the 2*H*-phenalene (B₃Z₂) and its analogous (B₂Z₂) molecule, as well as, for the B₅Z₃/B₄Z₃ and B₅Z₆/B₄Z₆ molecules.

When comparing the HOMA index results with those gathered from the NICS(1) and VIST calculations, a consistent agreement was observed among these tools in characterizing the aromaticity of individual rings. This agreement reinforces the general conclusions derived from the HOMA index. The phenalene isomers, B_3Z_m and B_2Z_m , present the same pattern for a given m. The NICS(1) values of the unsubstituted rings (A and C in Scheme 1) were closer to those of benzene for m=1, while for m=2, the NICS(1) values were smaller in absolute value.

In the case of the B_5Z_m systems, the m=1 exhibit four rings with high aromaticity, followed by m=2, 4, and 5, where two rings displayed higher aromaticity. For the biradical structure with m=3, only one VIST value, located at the outermost ring, was reasonably negative (-19.9 ppm). This correlates well with the location of the largest HOMA.

In conclusion, the comprehensive investigation conducted using aromaticity indexes, such as HOMA, NICS(1), and VIST, along with the reactivity analysis based on the low-lying excited states, the singlet-triplet energy separation, and the occupation of the natural orbitals calculated by multiconfigurational methodologies, revealed that the removal of sp^3 -carbon from three and five-rings molecules did not modify their π network, as initially anticipated. This fact may be of significant interest as these molecules could possess similar properties while offering alternative routes for more straightforward synthesis, thereby expanding the possibilities of starting materials and/or processes to construct organic semiconductors.

Supporting Information

The support information material contains the following information: Molecular structures of all studied systems (Scheme S1), natural frontier orbital plots of the phenalene isomers and π -electron analogs (Figure S1), NICSzz scans of the phenalene isomers and π -electron analogs (Figure S2),

28

natural frontier orbital plots of the olympicene isomers and π -electron analogs (Figure S3), NICSzz

scans of the olympicene isomers and π -electron analogs (Figure S4), adiabatic S-T energy separation

and main squared coefficient (Co^2) of the MR-AQCC wavefunction of the olympicene isomers and π -

electron analogs (Figure S5), ground and excited state configurations of the phenalene isomers and π -

electron analogs (Table S1), total and relative (adiabatic) electronic energies of phenalene and

olympicene isomers (Table S2), comparison of the total energies of the ground state and relative

energies of the excited states of the phenalene isomers using several methodologies (Table S3), Global

HOMA index of fused rings systems (Table S4), Cartesian coordinates and HOMA values of

phenalene isomers optimized with M06-2X/def2-TZVP, Cartesian coordinates of all studied structures

optimized with B3LYP/6-31G*.

Statements & Declarations

Funding

This work has been supported by Brazilian agencies Fundação de Amparo à Pesquisa do Estado

de São Paulo (FAPESP) under grants 2022/16385-86 and 2018/22669-3, 2019/03729-8, Conselho

Nacional de Desenvolvimento Científico e Tecnológico (CNPq) under grants 307168/2022-0,

313624/2019-4, 350437/2023-8 and 407124/2022-5. This study was financed in part by the

Coordenação de Aperfeiçoamento de Pessoal de Nível Superior - Brasil (CAPES) - Finance Code 001

under grants 88887.103153/2015-00 and 88882.447034/2019-01. HL acknowledges support from the

National Science Foundation under Grant No. 2107923. DN acknowledges support from the Czech

Science Foundation, projects 19-27454X.

Competing Interests

Financial interests: The authors declare they have no financial interests.

Data Availability

The datasets generated during the current study are available in the Supplementary Information.

Author Contributions

All authors contributed to the study conception and design. Data curation, and Validation were performed by Marcelo A.P. Pontes, Gabriel F.S. Fernandes, and Fernanda Bettanin. Conceptualization, Formal Analysis, Investigation, and Methodology were carried out by Fernanda Bettanin, Marcelo A.P. Pontes, and Luiz F.A. Ferrão. Funding acquisition, Resources were performed by Adélia J.A. Aquino, Hans Lischka, Dana Nachtigallova, Francisco B.C. Machado, and Luiz F.A. Ferrão. The first draft of the manuscript was written by Fernanda Bettanin, Marcelo A.P. Pontes, and Luiz F.A. Ferrão, and all authors commented on subsequent versions of the manuscript. All authors read and approved the final version of the manuscript.

References

- (1) Ratera, I.; Veciana, J. Playing with Organic Radicals as Building Blocks for Functional Molecular Materials. *Chem. Soc. Rev.* **2012**, *41* (1), 303–349. https://doi.org/10.1039/C1CS15165G.
- (2) Wang, Y.; Liu, B.; Koh, C. W.; Zhou, X.; Sun, H.; Yu, J.; Yang, K.; Wang, H.; Liao, Q.; Woo, H. Y.; et al. Facile Synthesis of Polycyclic Aromatic Hydrocarbon (PAH)—Based Acceptors with Fine-Tuned Optoelectronic Properties: Toward Efficient Additive-Free Nonfullerene Organic Solar Cells. *Adv Energy Mater* **2019**, *9* (24), 1–12. https://doi.org/10.1002/aenm.201803976.
- (3) Qin, T.; Wiedemair, W.; Nau, S.; Trattnig, R.; Sax, S.; Winkler, S.; Vollmer, A.; Koch, N.; Baumgarten, M.; List, E. J. W.; et al. Core, Shell, and Surface-Optimized Dendrimers for Blue Light-Emitting Diodes. *J Am Chem Soc* **2011**, *133* (5), 1301–1303. https://doi.org/10.1021/ja109734e.
- (4) Kim, S. K.; Yang, B.; Ma, Y.; Lee, J. H.; Park, J. W. Exceedingly Efficient Deep-Blue Electroluminescence from New Anthracenes Obtained Using Rational Molecular Design. *J Mater Chem* **2008**, *18* (28), 3376–3384. https://doi.org/10.1039/b805062g.
- (5) Gao, B.; Wang, M.; Cheng, Y.; Wang, L.; Jing, X.; Wang, F. Pyrazine-Containing Acene-Type Molecular Ribbons with up to 16 Rectilinearly Arranged Fused Aromatic Rings. *J Am Chem Soc* **2008**, *130* (26), 8297–8306. https://doi.org/10.1021/ja800311a.
- (6) Lin, Y.; Zhao, F.; He, Q.; Huo, L.; Wu, Y.; Parker, T. C.; Ma, W.; Sun, Y.; Wang, C.; Zhu, D.; et al. High-Performance Electron Acceptor with Thienyl Side Chains for Organic Photovoltaics. *J Am Chem Soc* **2016**, *138* (14), 4955–4961. https://doi.org/10.1021/jacs.6b02004.
- (7) Sun, Y.; Liu, Y.; Zhu, D. Advances in Organic Field-Effect Transistors. *J Mater Chem* **2005**, *15* (1), 53–65. https://doi.org/10.1039/b411245h.
- (8) Biermann, D.; Schmidt, W. Diels-Alder Reactivity of Polycyclic Aromatic Hydrocarbons. 1. Acenes and Benzologs. *J Am Chem Soc* **1980**, *102* (9), 3163–3173. https://doi.org/10.1021/ja00529a046.
- (9) Zhang, L.; Cao, Y.; Colella, N. S.; Liang, Y.; Brédas, J. L.; Houk, K. N.; Briseno, A. L. Unconventional, Chemically Stable, and Soluble Two-Dimensional Angular Polycyclic Aromatic Hydrocarbons: From Molecular Design to Device Applications. *Acc Chem Res* 2015, 48 (3), 500–509. https://doi.org/10.1021/ar500278w.
- (10) Xiang, Q.; Sun, Z. Doublet Open-Shell Graphene Fragments. *Chem Asian J* **2022**, *17* (13). https://doi.org/10.1002/asia.202200251.
- (11) Zhao, L.; Kaiser, R. I.; Lu, W.; Ahmed, M.; Oleinikov, A. D.; Azyazov, V. N.; Mebel, A. M.; Howlader, A. H.; Wnuk, S. F. Gas Phase Formation of Phenalene *via* 10π-Aromatic, Resonantly Stabilized Free Radical Intermediates. *Physical Chemistry Chemical Physics* 2020, 22 (27), 15381–15388. https://doi.org/10.1039/D0CP02216K.
- (12) Goto, K.; Kubo, T.; Yamamoto, K.; Nakasuji, K.; Sato, K.; Shiomi, D.; Takui, T.; Kubota, M.; Kobayashi, T.; Yakusi, K.; et al. A Stable Neutral Hydrocarbon Radical: Synthesis, Crystal Structure, and Physical Properties of 2,5,8-Tri- *Tert* -Butyl-Phenalenyl. *J Am Chem Soc* **1999**, *121* (7), 1619–1620. https://doi.org/10.1021/ja9836242.
- (13) Xiang, Q.; Guo, J.; Xu, J.; Ding, S.; Li, Z.; Li, G.; Phan, H.; Gu, Y.; Dang, Y.; Xu, Z.; et al. Stable Olympicenyl Radicals and Their π -Dimers. *J Am Chem Soc* **2020**, *142* (25), 11022–11031. https://doi.org/10.1021/jacs.0c02287.

- (14) Ravat, P.; Ribar, P.; Rickhaus, M.; Häussinger, D.; Neuburger, M.; Juríček, M. Spin-Delocalization in a Helical Open-Shell Hydrocarbon. *J Org Chem* **2016**, *81* (24), 12303–12317. https://doi.org/10.1021/acs.joc.6b02246.
- (15) Cui, Z.; Lischka, H.; Beneberu, H. Z.; Kertesz, M. Rotational Barrier in Phenalenyl Neutral Radical Dimer: Separating Pancake and van Der Waals Interactions. *J Am Chem Soc* **2014**, *136* (15), 5539–5542. https://doi.org/10.1021/ja412862n.
- (16) Mou, Z.; Uchida, K.; Kubo, T.; Kertesz, M. Evidence of σ and π -Dimerization in a Series of Phenalenyls. *J Am Chem Soc* **2014**, *136* (52), 18009–18022. https://doi.org/10.1021/ja509243p.
- (17) Cui, Z.; Lischka, H.; Beneberu, H. Z.; Kertesz, M. Double Pancake Bonds: Pushing the Limits of Strong π– π Stacking Interactions. J Am Chem Soc 2014, 136 (37), 12958–12965. https://doi.org/10.1021/ja505624y.
- (18) Tian, Y.-H.; Huang, J.; Kertesz, M. Fluxional σ-Bonds of 2,5,8-Tri-Tert-Butyl-1,3-Diazaphenalenyl Dimers: Stepwise [3,3], [5,5] and [7,7] Sigmatropic Rearrangements Viaπ-Dimer Intermediates. *Physical Chemistry Chemical Physics* **2010**, *12* (19), 5084. https://doi.org/10.1039/b925259b.
- (19) Shimizu, A.; Kubo, T.; Uruichi, M.; Yakushi, K.; Nakano, M.; Shiomi, D.; Sato, K.; Takui, T.; Hirao, Y.; Matsumoto, K.; et al. Alternating Covalent Bonding Interactions in a One-Dimensional Chain of a Phenalenyl-Based Singlet Biradical Molecule Having Kekulé Structures. *J Am Chem Soc* **2010**, *132* (41), 14421–14428. https://doi.org/10.1021/ja1037287.
- (20) Shimizu, A.; Uruichi, M.; Yakushi, K.; Matsuzaki, H.; Okamoto, H.; Nakano, M.; Hirao, Y.; Matsumoto, K.; Kurata, H.; Kubo, T. Resonance Balance Shift in Stacks of Delocalized Singlet Biradicals. *Angewandte Chemie International Edition* **2009**, *48* (30), 5482–5486. https://doi.org/10.1002/anie.200901382.
- (21) Huang, J.; Kertesz, M. Intermolecular Covalent π-π Bonding Interaction Indicated by Bond Distances, Energy Bands, and Magnetism in Biphenalenyl Biradicaloid Molecular Crystal. *J Am Chem Soc* 2007, 129
 (6), 1634–1643. https://doi.org/10.1021/ja066426g.
- (22) Pal, S. K.; Bag, P.; Sarkar, A.; Chi, X.; Itkis, M. E.; Tham, F. S.; Donnadieu, B.; Haddon, R. C. Hysteretic Spin and Charge Delocalization in a Phenalenyl-Based Molecular Conductor. *J Am Chem Soc* **2010**, *132* (48), 17258–17264. https://doi.org/10.1021/ja107201d.
- (23) Bag, P.; Itkis, M. E.; Pal, S. K.; Donnadieu, B.; Tham, F. S.; Park, H.; Schlueter, J. A.; Siegrist, T.; Haddon, R. C. Resonating Valence Bond and σ-Charge Density Wave Phases in a Benzannulated Phenalenyl Radical. *J Am Chem Soc* **2010**, *132* (8), 2684–2694. https://doi.org/10.1021/ja908768a.
- (24) Hicks, R. G. A New Spin on Bistability. *Nat Chem* **2011**, *3* (3), 189–191. https://doi.org/10.1038/nchem.997.
- (25) Haddon, R. C. Design of Organic Metals and Superconductors. *Nature* **1975**, *256* (5516), 394–396. https://doi.org/10.1038/256394a0.
- (26) Morita, Y.; Suzuki, S.; Sato, K.; Takui, T. Synthetic Organic Spin Chemistry for Structurally Well-Defined Open-Shell Graphene Fragments. *Nat Chem* **2011**, *3* (3), 197–204. https://doi.org/10.1038/nchem.985.
- (27) Ravat, P.; Blacque, O.; Juríček, M. Benzo[*Cd*]Triangulene: A Spin 1/2 Graphene Fragment. *J Org Chem* **2020**, *85* (1), 92–100. https://doi.org/10.1021/acs.joc.9b02163.
- (28) Kubo, T. Phenalenyl-Based Open-Shell Polycyclic Aromatic Hydrocarbons. *The Chemical Record* **2015**, 15 (1), 218–232. https://doi.org/10.1002/tcr.201402065.

- (29) Murata, I.; Nakazawa, T.; Okazaki, M. 2-Ethoxy-9,10,11,12-Tetrachloropentaphenafulvalene. *Tetrahedron Lett* **1969**, *10* (24), 1921–1924. https://doi.org/10.1016/S0040-4039(01)88047-3.
- (30) Nakasuji, Kazuhiro.; Yamaguchi, Masakazu.; Murata, Ichiro.; Nakanishi, Hiroshi. First Realization of 3-Fold Fluxionality in Polycyclic Conjugated Hydrocarbon-Metal Complexes: Synthesis and Dynamic NMR Study of [Pd(.Eta.3-Phenalenyl)(Tmeda)]+PF6- and Its Methyl Derivative. *J Am Chem Soc* **1986**, *108* (2), 325–327. https://doi.org/10.1021/ja00262a039.
- (31) Uchida, K.; Kubo, T. Recent Advances in the Chemistry of Phenalenyl. *Journal of Synthetic Organic Chemistry, Japan* **2016**, *74* (11), 1069–1077. https://doi.org/10.5059/yukigoseikyokaishi.74.1069.
- (32) Chi, X.; Itkis, M. E.; Patrick, B. O.; Barclay, T. M.; Reed, R. W.; Oakley, R. T.; Cordes, A. W.; Haddon, R. C. The First Phenalenyl-Based Neutral Radical Molecular Conductor. *J Am Chem Soc* **1999**, *121* (44), 10395–10402. https://doi.org/10.1021/ja992040c.
- (33) Chi, X.; Itkis, M. E.; Kirschbaum, K.; Pinkerton, A. A.; Oakley, R. T.; Cordes, A. W.; Haddon, R. C. Dimeric Phenalenyl-Based Neutral Radical Molecular Conductors. *J Am Chem Soc* **2001**, *123* (17), 4041–4048. https://doi.org/10.1021/ja0039785.
- (34) Itkis, M. E.; Chi, X.; Cordes, A. W.; Haddon, R. C. Magneto-Opto-Electronic Bistability in a Phenalenyl-Based Neutral Radical. *Science* (1979) **2002**, 296 (5572), 1443–1445. https://doi.org/10.1126/science.1071372.
- (35) Banik, A.; Mandal, S. K. Tuning Redox States of Phenalenyl-Based Molecules by Consecutive Reduction toward Transition Metal-Free Heck-Type C–C Cross-Coupling. *ACS Catal* **2022**, *12* (9), 5000–5012. https://doi.org/10.1021/acscatal.2c00173.
- (36) Reddoch, A. H.; Paskovich, D. H. The EPR Spectrum of Benzo [Cd] Pyrenyl. *Chem Phys Lett* **1969**, *3* (6), 351–352. https://doi.org/10.1016/0009-2614(69)80133-8.
- (37) Nowakowski, J. On the Assignment of Proton Hyperfine Splitting Constants in Benzo[Cd]Pyrenyl. *Chem Phys Lett* **1972**, *13* (6), 589–591. https://doi.org/10.1016/0009-2614(72)85020-6.
- (38) Mistry, A.; Moreton, B.; Schuler, B.; Mohn, F.; Meyer, G.; Gross, L.; Williams, A.; Scott, P.; Costantini, G.; Fox, D. J. The Synthesis and STM/AFM Imaging of 'Olympicene' Benzo[*Cd*]Pyrenes. *Chemistry A European Journal* **2015**, *21* (5), 2011–2018. https://doi.org/10.1002/chem.201404877.
- (39) Yildirim, H.; Kara, A. Effect of van Der Waals Interactions on the Adsorption of Olympicene Radical on Cu(111): Characteristics of Weak Physisorption versus Strong Chemisorption. *The Journal of Physical Chemistry C* 2013, 117 (6), 2893–2902. https://doi.org/10.1021/jp311361e.
- (40) Schuler, B.; Liu, W.; Tkatchenko, A.; Moll, N.; Meyer, G.; Mistry, A.; Fox, D.; Gross, L. Adsorption Geometry Determination of Single Molecules by Atomic Force Microscopy. *Phys Rev Lett* **2013**, *111* (10), 106103. https://doi.org/10.1103/PhysRevLett.111.106103.
- (41) Liu, W.; Tkatchenko, A.; Scheffler, M. Modeling Adsorption and Reactions of Organic Molecules at Metal Surfaces. *Acc Chem Res* **2014**, *47* (11), 3369–3377. https://doi.org/10.1021/ar500118y.
- (42) Yildirim, H.; Matos, J.; Kara, A. Role of Long-Range Interactions for the Structure and Energetics of Olympicene Radical Adsorbed on Au(111) and Pt(111) Surfaces. *The Journal of Physical Chemistry C* **2015**, *119* (45), 25408–25419. https://doi.org/10.1021/acs.jpcc.5b08191.
- (43) Feng, L.; Zhang, W. X. The Structure and Magnetism of Graphone. *AIP Adv* **2012**, *2* (4), 042138. https://doi.org/10.1063/1.4766937.

- (44) Lee, C.; Leconte, N.; Kim, J.; Cho, D.; Lyo, I.-W.; Choi, E. J. Optical Spectroscopy Study on the Effect of Hydrogen Adsorption on Graphene. *Carbon N Y* **2016**, *103*, 109–114. https://doi.org/10.1016/j.carbon.2016.03.008.
- (45) Zhou, J.; Wu, M. M.; Zhou, X.; Sun, Q. Tuning Electronic and Magnetic Properties of Graphene by Surface Modification. *Appl Phys Lett* **2009**, *95* (10), 103108. https://doi.org/10.1063/1.3225154.
- (46) Hornekær, L.; Rauls, E.; Xu, W.; Šljivančanin, Ž.; Otero, R.; Stensgaard, I.; Lægsgaard, E.; Hammer, B.; Besenbacher, F. Clustering of Chemisorbed H(D) Atoms on the Graphite (0001) Surface Due to Preferential Sticking. *Phys Rev Lett* **2006**, *97* (18), 186102. https://doi.org/10.1103/PhysRevLett.97.186102.
- (47) Skov, A. L.; Thrower, J. D.; Hornekær, L. Polycyclic Aromatic Hydrocarbons Catalysts for Molecular Hydrogen Formation. *Faraday Discuss.* **2014**, *168*, 223–234. https://doi.org/10.1039/C3FD00151B.
- (48) Schneiker, A.; Csonka, I. P.; Tarczay, G. Hydrogenation and Dehydrogenation Reactions of the Phenalenyl Radical/1H-Phenalene System at Low Temperatures. *Chem Phys Lett* **2020**, *743*, 137183. https://doi.org/10.1016/j.cplett.2020.137183.
- (49) Zoellner, J. M.; Zoellner, R. W. The Isomers of Phenalene and Their Singlet and Triplet States: A Hartree– Fock and Density Functional Computational Investigation. *Journal of Molecular Structure: THEOCHEM* 2008, 863 (1–3), 50–54. https://doi.org/10.1016/j.theochem.2008.05.017.
- (50) O'Connor, G. D.; Chan, B.; Sanelli, J. A.; Cergol, K. M.; Dryza, V.; Payne, R. J.; Bieske, E. J.; Radom, L.; Schmidt, T. W. Hydrogen-Adduction to Open-Shell Graphene Fragments: Spectroscopy, Thermochemistry and Astrochemistry. *Chem Sci* **2017**, *8* (2), 1186–1194. https://doi.org/10.1039/C6SC03787A.
- (51) Lock, G.; Gergely, G. Über Perinaphthinden. *Berichte der deutschen chemischen Gesellschaft (A and B Series)* **1944**, 77 (6–7), 461–465. https://doi.org/10.1002/cber.19440770617.
- (52) Valentine, A. J. S.; Mazziotti, D. A. Theoretical Prediction of the Structures and Energies of Olympicene and Its Isomers. *J Phys Chem A* **2013**, *117* (39), 9746–9752. https://doi.org/10.1021/jp312384b.
- (53) Günther, K.; Grabicki, N.; Battistella, B.; Grubert, L.; Dumele, O. An All-Organic Photochemical Magnetic Switch with Bistable Spin States. *J Am Chem Soc* **2022**, *144* (19), 8707–8716. https://doi.org/10.1021/jacs.2c02195.
- (54) Ravat, P.; Šolomek, T.; Häussinger, D.; Blacque, O.; Juríček, M. Dimethylcethrene: A Chiroptical Diradicaloid Photoswitch. *J Am Chem Soc* **2018**, *140* (34), 10839–10847. https://doi.org/10.1021/jacs.8b05465.
- (55) Bally, T.; Zhu, Z.; Wirz, J.; Fülscher, M.; Hasegawa, J.-Y. Radical Cations of Perinaphthocyclopropanes. Conditions for the Observation of 1,3-Perinaphthadiyl Radical Cations†. *Journal of the Chemical Society, Perkin Transactions 2* **2000**, No. 11, 2311–2318. https://doi.org/10.1039/b002808h.
- (56) Bearpark, M. J.; Boggio-Pasqua, M. Excited States of Conjugated Hydrocarbon Radicals Using the Molecular Mechanics Valence Bond (MMVB) Method. *Theoretical Chemistry Accounts: Theory, Computation, and Modeling (Theoretica Chimica Acta)* **2003**, *110* (2), 105–114. https://doi.org/10.1007/s00214-003-0461-3.
- (57) Fulara, J.; Chakraborty, A.; Maier, J. P. Electronic Characterization of Reaction Intermediates: The Fluorenylium, Phenalenylium, and Benz[f]Indenylium Cations and Their Radicals. *Angewandte Chemie International Edition* **2016**, *55* (10), 3424–3427. https://doi.org/10.1002/anie.201511230.

- (58) Dominikowska, J.; Domagala, M.; Palusiak, M. UV-Vis Spectra of Singlet State Cationic Polycyclic Aromatic Hydrocarbons: Time-Dependent Density Functional Theory Study. *J Chem Phys* **2014**, *140* (4), 044324. https://doi.org/10.1063/1.4862902.
- (59) Fortenberry, R. C.; Moore, M. M.; Lee, T. J. Excited State Trends in Bidirectionally Expanded Closed-Shell PAH and PANH Anions. *J. Phys Chem A* **2016**, *120* (37), 7327–7334. https://doi.org/10.1021/acs.jpca.6b06654.
- (60) Solà, M. Forty Years of Clar's Aromatic π -Sextet Rule. Front Chem **2013**, 1 (October), 4–11. https://doi.org/10.3389/fchem.2013.00022.
- (61) Clar, E. The Aromatic Sextet. In *Mobile Source Emissions Including Policyclic Organic Species*; Springer Netherlands: Dordrecht, 1983; pp 49–58. https://doi.org/10.1007/978-94-009-7197-4_4.
- (62) Stephens, P.; Devlin, F. J.; Chabalowski, C. F.; Frisch, M. J. Ab-Initio Calculation of Vibrational Absorption and Circular-Dichroism Spectra Using Density-Functional Force-Fields. *Journal Of Physical Chemistry* **1994**, *98* (45), 11623–11627. https://doi.org/10.1021/j100046a014.
- (63) Hehre, W. J.; Ditchfield, R.; Pople, J. A. Self—Consistent Molecular Orbital Methods. XII. Further Extensions of Gaussian—Type Basis Sets for Use in Molecular Orbital Studies of Organic Molecules. *J Chem Phys* **1972**, *56* (5), 2257–2261. https://doi.org/10.1063/1.1677527.
- (64) Hariharan, P. C.; Pople, J. A. The Influence of Polarization Functions on Molecular Orbital Hydrogenation Energies. *Theor Chim Acta* **1973**, *28* (3), 213–222. https://doi.org/10.1007/BF00533485.
- (65) Zhao, Y.; Truhlar, D. G. The M06 Suite of Density Functionals for Main Group Thermochemistry, Thermochemical Kinetics, Noncovalent Interactions, Excited States, and Transition Elements: Two New Functionals and Systematic Testing of Four M06-Class Functionals and 12 Other Function. *Theor Chem Acc* 2008, 120 (1–3), 215–241. https://doi.org/10.1007/s00214-007-0310-x.
- (66) Weigend, F.; Ahlrichs, R. Balanced Basis Sets of Split Valence, Triple Zeta Valence and Quadruple Zeta Valence Quality for H to Rn: Design and Assessment of Accuracy. *Physical Chemistry Chemical Physics* **2005**, *7* (18), 3297. https://doi.org/10.1039/b508541a.
- (67) Weigend, F. Accurate Coulomb-Fitting Basis Sets for H to Rn. *Physical Chemistry Chemical Physics* **2006**, 8 (9), 1057. https://doi.org/10.1039/b515623h.
- (68) Krygowski, T. M.; Cyrański, M. K. Structural Aspects of Aromaticity. *Chem Rev* **2001**, *101* (5), 1385–1420. https://doi.org/10.1021/cr990326u.
- (69) Cunha, L. A.; Pinheiro Jr, M. *PyCRAI Color Rings by Aromaticity Index*. https://github.com/maxjr82/PyCRAI
- (70) Milanez, B. D.; Chagas, J. C. V.; Pinheiro Jr, M.; Aquino, A. J. A.; Lischka, H.; Machado, F. B. C. Effects on the Aromaticity and on the Biradicaloid Nature of Acenes by the Inclusion of a Cyclobutadiene Linkage. *Theor Chem Acc* **2020**, *139* (7), 113. https://doi.org/10.1007/s00214-020-02624-w.
- (71) Plasser, F. Exploitation of Baird Aromaticity and Clar's Rule for Tuning the Triplet Energies of Polycyclic Aromatic Hydrocarbons. *Chemistry (Easton)* **2021**, *3* (2), 532–549. https://doi.org/10.3390/chemistry3020038.
- (72) Stanger, A. Nucleus-Independent Chemical Shifts (NICS): Distance Dependence and Revised Criteria for Aromaticity and Antiaromaticity. *J Org Chem* **2006**, *71* (3), 883–893. https://doi.org/10.1021/jo051746o.

- (73) Stanger, A. Obtaining Relative Induced Ring Currents Quantitatively from NICS. *J Org Chem* **2010**, *75* (7), 2281–2288. https://doi.org/10.1021/jo1000753.
- (74) Plasser, F.; Glöcklhofer, F. Visualisation of Chemical Shielding Tensors (VIST) to Elucidate Aromaticity and Antiaromaticity**. *European J Org Chem* **2021**, *2021* (17), 2529–2539. https://doi.org/10.1002/ejoc.202100352.
- (75) Plasser, F. TheoDORE: A Toolbox for a Detailed and Automated Analysis of Electronic Excited State Computations. *Journal of Chemical Physics* **2020**, *152* (8). https://doi.org/10.1063/1.5143076.
- (76) Szalay, P. G.; Bartlett, R. J. Multi-Reference Averaged Quadratic Coupled-Cluster Method: A Size-Extensive Modification of Multi-Reference Cl. *Chem Phys Lett* **1993**, *214* (5), 481–488. https://doi.org/10.1016/0009-2614(93)85670-J.
- (77) Werner, H. H.-J.; Knowles, P. J. A Second Order Multiconfiguration SCF Procedure with Optimum Convergence. *J Chem Phys* **1985**, *82* (11), 5053. https://doi.org/10.1063/1.448627.
- (78) Bettanin, F.; Ferrão, L. F. A.; Pinheiro, M.; Aquino, A. J. A.; Lischka, H.; Machado, F. B. C.; Nachtigallova,
 D. Singlet L_a and L_b Bands for N-Acenes (N = 2-7): A CASSCF/CASPT2 Study. *J Chem Theory Comput* 2017, 13 (9), 4297–4306. https://doi.org/10.1021/acs.jctc.7b00302.
- (79) Finley, J.; Malmqvist, P.-Å.; Roos, B. O.; Serrano-Andrés, L. The Multi-State CASPT2 Method. *Chem Phys Lett* **1998**, *288* (2–4), 299–306. https://doi.org/10.1016/S0009-2614(98)00252-8.
- (80) Celani, P.; Werner, H.-J. Multireference Perturbation Theory for Large Restricted and Selected Active Space Reference Wave Functions. *J Chem Phys* **2000**, *112* (13), 5546–5557. https://doi.org/10.1063/1.481132.
- (81) Shiozaki, T.; Győrffy, W.; Celani, P.; Werner, H.-J. Communication: Extended Multi-State Complete Active Space Second-Order Perturbation Theory: Energy and Nuclear Gradients. *J Chem Phys* **2011**, *135* (8), 081106-1-081106-4. https://doi.org/10.1063/1.3633329.
- (82) Shiozaki, T.; Werner, H.-J. Communication: Second-Order Multireference Perturbation Theory with Explicit Correlation: CASPT2-F12. *J Chem Phys* **2010**, *133* (14), 141103-1-141103—141104. https://doi.org/10.1063/1.3489000.
- (83) Andersson, Kerstin.; Malmqvist, P. Aake.; Roos, B. O.; Sadlej, A. J.; Wolinski, Krzysztof. Second-Order Perturbation Theory with a CASSCF Reference Function. *J Phys Chem* **1990**, *94* (14), 5483–5488. https://doi.org/10.1021/j100377a012.
- (84) Roos, B. O.; Linse, P.; Siegbahn, P. E. M.; Blomberg, M. R. a. A Simple Method for the Evaluation of the Second-Order-Perturbation Energy from External Double-Excitations with a CASSCF Reference Wavefunction. *Chem Phys* **1982**, *66* (1–2), 197–207. https://doi.org/10.1016/0301-0104(82)88019-1.
- (85) Roos, B. O.; Andersson, K. Multiconfigurational Perturbation Theory with Level Shift the Cr2 Potential Revisited. *Chem Phys Lett* **1995**, *245* (2), 215–223. https://doi.org/https://doi.org/10.1016/0009-2614(95)01010-7.
- (86) Frisch, M. J.; Trucks, G. W.; Schlegel, H. B.; Scuseria, G. E.; Robb, M. A.; Cheeseman, J. R.; Scalmani, G.; Barone, V.; Mennucci, B.; Petersson, G. A.; et al. Gaussian 09, Revision B.01. Gaussian, Inc.: Wallingford CT 2010.

- (87) Werner, H.-J.; Knowles, P. J.; Knizia, G.; Manby, F. R.; Schütz, M. Molpro: A General-Purpose Quantum Chemistry Program Package. *Wiley Interdiscip Rev Comput Mol Sci* **2012**, *2* (2), 242–253. https://doi.org/10.1002/wcms.82.
- (88) Werner, H.-J.; Knowles, P. J.; Knizia, G.; Manby, F. R.; Schütz, M.; others. MOLPRO, Version 2015.1, a Package of Ab Initio Programs. Cardiff, UK 2015.
- (89) Karadakov, P. B.; Horner, K. E. Magnetic Shielding in and around Benzene and Cyclobutadiene: A Source of Information about Aromaticity, Antiaromaticity, and Chemical Bonding. *J Phys Chem A* **2013**, *117* (2), 518–523. https://doi.org/10.1021/jp311536c.
- (90) Karadakov, P. B. Magnetic Shielding Study of Bonding and Aromaticity in Corannulene and Coronene. *Chemistry (Easton)* **2021**, *3* (3), 861–872. https://doi.org/10.3390/chemistry3030063.
- (91) Herzberg, G. Molecular Spectra and Molecular Structure. Vol. 3: Electronic Spectra and Electronic Structure of Polyatomic Molecules; 1966; Vol. 1.
- (92) Fawcett, J. K.; Trotter, J. The Crystal and Molecular Structure of Coronene. *Proc R Soc Lond A Math Phys Sci* **1966**, *289* (1418), 366–376.
- (93) Arpa, E. M.; Durbeej, B. HOMER: A Reparameterization of the Harmonic Oscillator Model of Aromaticity (HOMA) for Excited States. *Physical Chemistry Chemical Physics* **2023**, *25* (25), 16763–16771. https://doi.org/10.1039/D3CP00842H.

TOC Graphic

